

# Measurement of the Absolute np Scattering Differential Cross Section at 194 MeV

M. Sarsour<sup>1</sup>, T. Peterson<sup>1,\*</sup>, M. Planinic<sup>1,†</sup>, S.E. Vigdor<sup>1</sup>, C. Allgower<sup>1</sup>, B. Bergenwall<sup>2</sup>, J. Blomgren<sup>2</sup>, T. Hossbach<sup>1</sup>, W.W. Jacobs<sup>1</sup>, C. Johansson<sup>2</sup>, J. Klug<sup>2</sup>, A.V. Klyachko<sup>1</sup>, P. Nadel-Turonski<sup>2</sup>, L. Nilsson<sup>2</sup>, N. Olsson<sup>2</sup>, S. Pomp<sup>2</sup>, J. Rapaport<sup>3</sup>, T. Rinckel<sup>1</sup>, E.J. Stephenson<sup>1</sup>, U. Tippawan<sup>2,4</sup>, S.W. Wissink<sup>1</sup>, and Y. Zhou<sup>1</sup>

<sup>1</sup>*Indiana University Cyclotron Facility and Department of Physics,  
Bloomington, IN 47408, USA*

<sup>2</sup>*Uppsala University, Uppsala, Sweden*

<sup>3</sup>*Ohio University, Athens, OH, USA*

<sup>4</sup>*Chiang Mai University, Chiang Mai, Thailand*

(Dated: September 30, 2018)

We describe a double-scattering experiment with a novel tagged neutron beam to measure differential cross sections for np back-scattering to better than  $\pm 2\%$  absolute precision. The measurement focuses on angles and energies where the cross section magnitude and angle-dependence constrain the charged pion-nucleon coupling constant, but existing data show serious discrepancies among themselves and with energy-dependent partial wave analyses (PWA). The present results are in good accord with the PWA, but deviate systematically from other recent measurements.

PACS numbers: 25.40.Dn, 25.10.+s, 28.20.Cz

The neutron-proton elastic scattering database at intermediate energies is plagued by experimental inconsistencies and cross section normalization difficulties [1, 2, 3]. These problems have led the most sophisticated partial wave analyses (PWA) of the data [4, 5, 6] to ignore the majority (including the most recent) of measured cross sections, while the literature is filled with heated debates over experimental and theoretical methods [7, 8], including proposed radical “doctoring” (angle-dependent renormalization) to “salvage” allegedly flawed data [9]. Meanwhile, an empirical evaluation of a fundamental parameter of meson-exchange theories of the nuclear force – the charged  $\pi NN$  coupling constant,  $f_c^2$  – hangs in the balance [8]. We report here the results of a new experiment, carried out utilizing quite different techniques from earlier measurements in an attempt to resolve the most worrisome experimental discrepancies.

The present experiment involves a kinematically complete double-scattering measurement to produce and utilize a “tagged” intermediate-energy neutron beam [10], thus greatly reducing the usual systematic uncertainties associated with the determination of neutron flux. Products from the second scattering were detected over the full angle range of interest simultaneously in a large-acceptance detector array, to eliminate the need for cross-normalization of different regions of the angular distribution. The use of carefully matched solid  $\text{CH}_2$  and C targets permitted frequent measurement and accurate subtraction of quasifree scattering background, thereby minimizing reliance on kinematic cuts to isolate the free np-scattering sample. These methods, combined with multiple internal crosschecks built into the data analysis procedures, have allowed us to achieve systematic error levels in the absolute cross section below 2%. In addition to addressing the previous discrepancies, the re-

sults provide a useful absolute cross section calibration for intermediate-energy neutron-induced reactions.

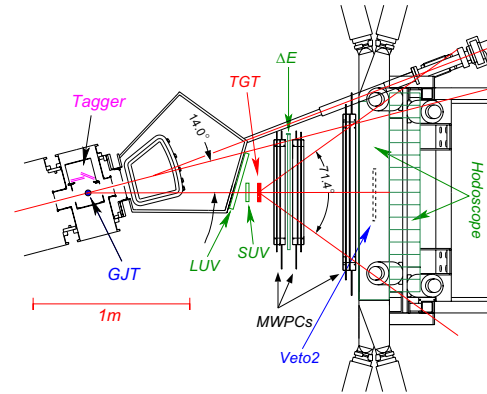


FIG. 1: Top view of the np scattering experiment setup.

The experiment was carried out during the final year of operation of the Indiana University Cyclotron Facility’s Cooler ring [11], with apparatus illustrated in Fig. 1 and described in detail in [10]. Neutrons of 185-197 MeV were produced via the charge-exchange reaction  $p+d \rightarrow n+2p$ , initiated by a stored, electron-cooled 203 MeV proton beam, with typical circulating current of 1-2 mA, in a windowless deuterium gas jet target (GJT) of thickness  $\approx 2 - 4 \times 10^{15}$  atoms/cm<sup>2</sup>. The ultra-thin target permitted detection of the two low-energy recoil protons in an array (“tagger” in Fig. 1) of four  $6.4 \times 6.4$  cm<sup>2</sup> double-sided silicon strip detectors (DSSD) with 480  $\mu\text{m}$  readout pitch in two orthogonal directions, each followed by a silicon pad (“backing”) detector (BD) of the same area. Only recoil protons ( $\lesssim 11$  MeV) that stopped in either the DSSD’s or BD’s were considered in the data analysis. Measurements of energy, arrival time, and two-dimensional position for both recoil protons in the tagger,

when combined with precise knowledge of cooled p beam direction and energy, allowed 4-momentum determination for each produced neutron on an event-by-event basis. The (uncollimated) tagged neutrons were distributed over a significant range in energy and angle, but these parameters were measured for each produced neutron with resolutions  $\sigma_E \approx 60$  keV and  $\sigma_{angle} \approx 2$  mrad.

The forward setup included a solid secondary scattering target of CH<sub>2</sub> or graphite positioned 1.1 m downstream of the GJT, centered on a neutron production lab angle of 14.0°. Both solid targets had transverse dimensions 20×20 cm<sup>2</sup> and thickness of  $0.99 \times 10^{23}$  carbon atoms/cm<sup>2</sup>. The typical flux of tagged neutrons with energy above 185 MeV intercepting the secondary target was 200 Hz. Two upstream plastic scintillators (LUV and SUV in Fig. 1) vetoed tagged neutrons that interacted before the secondary target. Following the target was a forward array of plastic scintillators for triggering and energy information and a set of three (3-plane) multi-wire proportional chambers (MWPCs) to track forward protons. The forward detector acceptance was nearly 100% for np scattering events with  $\theta_{c.m.} \geq 130^\circ$ , falling to 50% by  $\theta_{c.m.} = 90^\circ$ . The MWPC between the secondary target and  $\Delta E$  scintillator allowed discrimination against np events initiated in that scintillator. The rear hodoscope comprised 20 plastic scintillator bars of sufficient thickness (20 cm) to stop 200 MeV protons and give 15-20% detection efficiency for 100-200 MeV neutrons.

Specially designed DSSD front-end electronics [10] permitted a tagger-based event trigger on neutron candidates (consistent with two distinct tagger hits and no accompanying signals from LUV or SUV), whether or not the neutrons interacted in the forward target and/or detectors. Tagged neutron events were recorded in three mutually exclusive event streams [10], coupling the tagger trigger with (1) no rear hodoscope coincidence (providing a prescaled sample for neutron flux monitoring); or a coincidence with (2) both  $\Delta E$  scintillator and rear hodoscope (for np scattering candidates); or (3) rear hodoscope but not  $\Delta E$  (for evaluating the neutron detection efficiency of the hodoscope). Comparative analyses of the three separate event streams, with respective yields  $N_1$ ,  $N_2$  and  $N_3$ , facilitated crosschecks to calibrate the system [10] and to study potential systematic errors.

Neutron beam properties were defined by identical cuts for all three event streams, so that associated systematic uncertainties would cancel in the yield ratios from which the absolute np scattering cross section is extracted. Among the common cuts are ones on DSSD vs. BD energy deposition in the tagger [10], used to select two tagged neutron classes for analysis: (a) “2-stop” events, where both recoil protons stopped inside the DSSD’s (either the same or different quadrants of the tagger); (b) “1-punch” events, where one of two recoil protons incident on different quadrants punched through into the corresponding BD and stopped there. These classes differ

significantly in neutron energy ( $E_n$ ) and position profiles [10], allowing an important crosscheck on the accuracy of the tagging technique by comparing np cross sections extracted independently from each class. Other common cuts defined a fiducial area for neutrons impinging on the secondary target and eliminated common-mode BD noise (via pulse height correlations among quadrants) that sometimes led to misidentification of event class.

Additional misidentification discovered during data analysis was attributed to an electronics malfunction in the gating or clearing circuit for one analog-to-digital converter module, that removed all valid BD energy signals for some fraction of events. The corrupted events were misidentified as 2-stop events, with systematically incorrect predictions of tagged neutron trajectory (since some recoil proton energy was missed), and hence of np scattering angle for event stream 2. A subsample of these corrupted events could be isolated by means of their valid BD timing signals, and their properties were accurately reproduced by appropriately scaling the surviving sample of all events with valid BD energies and times, after setting these energies to zero in software. Thus, the surviving punch-through events permitted a reliably unbiased subtraction of the corrupted 2-stop events, independently for each event stream. The subtraction confirmed that the same fraction (typically 23%) of punch-through events was lost from each event stream, with no net effect on the extracted 1-punch cross sections.

Kinematic cuts applied exclusively to event stream 2 to define np free-scattering events from the secondary target were used sparingly. We relied instead on accurate background subtraction facilitated by frequent interchange of the carefully matched CH<sub>2</sub> and C targets. The CH<sub>2</sub> and C runs were normalized via the pd elastic scattering yield from the GJT measured in a fourth event stream for the two targets. The pd events were identified by their clear kinematic locus in the energy of recoil deuterons detected in the tagger *vs.* the position of coincident forward protons in the front MWPC. The subtraction removed not only quasifree scattering off carbon nuclei in the target, but also background from other sources, such as tagged n scattering from the aluminum support platform on which the secondary target sat, or protons produced in the GJT that passed above the top of the LUV and SUV scintillators, mocking up np back-scattering events.

The success of the background subtraction is illustrated in Fig. 2, where (a) and (b) show the vertical position ( $y_{tag}$ ) of neutrons on the secondary target, as reconstructed from the tagger, for CH<sub>2</sub> and normalized C targets, and for their difference. Figure 2(c) shows the  $\Delta E$  pulse-height spectrum within a given scattering angle ( $\theta_p^{sc}$ ) bin for both targets and for their difference. Prominent background features associated both with the secondary target (*e.g.*, the long quasifree scattering tail in  $\Delta E$ ) and with other sources (*e.g.*, the peak in frame (a) from the Al support platform) are simultaneously ac-

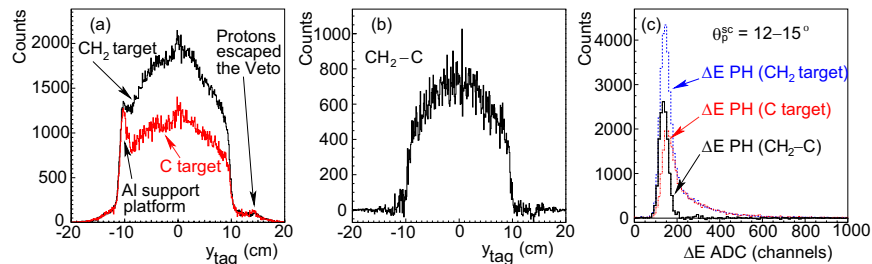


FIG. 2: Distributions of np scattering candidate events in  $y_{tag}$  (a,b) and  $\Delta E$  (c) for  $\text{CH}_2$  and C targets and their difference.

curately removed by the subtraction. The subtraction reveals in frame (b) a  $y_{tag}$  distribution reflecting the tagged n (2-stop + 1-punch) beam profile, convoluted with the np scattering cross section, forward detector acceptance and sharp  $\text{CH}_2$  target edges (the sharpness illustrating the good spatial resolution of the tagging).

Background-subtracted spectra such as that in Fig. 2(c) were used to evaluate efficiencies for the few loose cuts imposed on event stream 2 to improve the free-scattering signal-to-background ratio, including ones on  $\Delta E$  vs.  $\theta_p^{sc}$  and on MWPC proton track quality. Cuts on the hodoscope pulse height were avoided, to remove reliance on detailed understanding of the nuclear reaction tail for protons stopping in this thick scintillator.

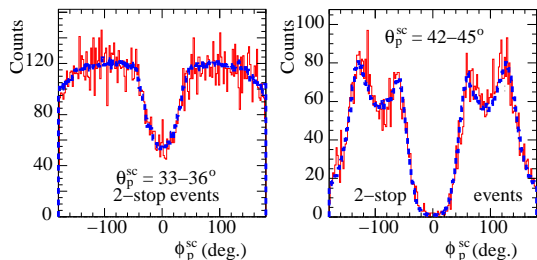


FIG. 3: The distribution of free ( $\text{CH}_2\text{-C}$ ) np scattering events with respect to proton azimuthal angle  $\phi$ , for two lab scattering angle bins. The solid (dashed) histograms are measured (simulated and normalized to fit the measurements).

The forward detector acceptance was determined as a function of  $\theta_p^{sc}$  from simulations matched to *measured* distributions of np free-scattering events in proton azimuthal angle  $\phi_p$ . In the simulations, the longitudinal coordinate of the n production vertex within the GJT and its transverse coordinates on the secondary target were generated randomly for each event, but within distributions determined from the experiment. These coordinates determined the incident n angle. Generated outgoing p trajectories were accepted if they would yield signals above the hodoscope threshold (required in trigger) and in all three MWPCs (required in the data analysis). Forward detector location parameters were tuned to reproduce the measured  $\phi_p$  distributions for all  $\theta_p^{sc}$  bins and for 1-punch and 2-stop samples simultaneously.

Typical fits in Fig. 3 reveal structure of purely geometric origin, from rectangular detector edges projected on  $\theta$  and  $\phi$ . For  $\theta_p^{sc} \leq 24^\circ$  the measured and simulated  $\phi$  distributions are uniform, since the scattered protons are completely contained within the forward array.

Absolute differential cross sections were obtained from the yields in event streams 1, 2 and 3 defined above:

$$\left(\frac{d\sigma}{d\Omega}\right)_{lab} = \frac{N_2(\theta_p^{sc}) \prod c_i}{(N_1 + N_2 + N_3) t_H |d \cos(\theta_p^{sc})| a_\phi(\theta_p^{sc})}, \quad (1)$$

where  $N_j$  represents the number of events (corrected for prescaling where appropriate) surviving all relevant cuts and background subtractions for event stream  $j$ ; the  $c_i$  are small corrections, summarized in Table I, for inefficiencies, tagged neutron losses or backgrounds, and software cut and dead time differences among event streams;  $t_H = (1.988 \pm 0.008) \times 10^{23}$  H atoms/cm<sup>2</sup> for the  $\text{CH}_2$  target; and  $a_\phi$  is the azimuthal acceptance determined from simulations for the given angle bin. The data were analyzed in 1 MeV wide  $E_n$  slices from 185 to 197 MeV, and among the  $c_i$  for each slice are small (always < 1%) corrections, based on the theoretical energy dependence calculated with the Nijmegen PWA [4], to extract an effective cross section at  $\langle E_n \rangle = 194.0 \pm 0.15$  MeV.

Cross sections extracted independently for the 1-punch and 2-stop samples agree within statistical uncertainties ( $\chi^2/\text{point} \approx 1.0$ ) in both magnitude and angular shape. This comparison supports the reliability of the experiment and analysis, as these events come from complementary regions of the tagged beam spatial and energy profiles [10]. Cross sections extracted for different time periods within the production runs, and with different sets of cuts, are also consistent within uncertainties. The results, averaged over the 2-stop and 1-punch samples, are compared in Fig. 4 with previous experimental results at 162 MeV [3] and with the Nijmegen partial wave analysis (PWA93) at the two relevant energies [13].

By using a tagged beam, we have sacrificed statistical precision for better control of systematic errors, in order to assess which previous experiments may have suffered from unrecognized systematic problems. Each systematic uncertainty summarized in Table I has been evaluated in a separate analysis, sometimes involving auxiliary measurements. The errors are, except where noted otherwise

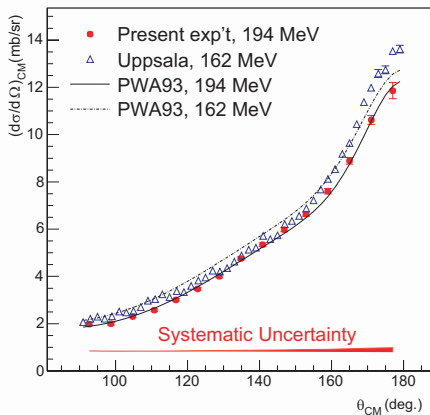


FIG. 4: Absolute differential cross section from the present experiment, compared with data from Ref. [3] and with PWA calculations at two relevant energies. The error bars and shaded band for the present results represent, respectively, statistical (including background subtraction) and systematic (including overall normalization) uncertainties.

in the Table, angle-independent normalization uncertainties. The largest correction to the data and attendant uncertainty arise from cuts to remove stream 2 (but not 1 or 3) events where the np scattering vertex transverse coordinates predicted from n tagging *vs.* p ray-tracing disagree by more than three times the resolution  $\sigma$ . The removed events (6.3% of the total sample) are affected by several factors – *e.g.*, sequential reactions in the secondary target and upstream material, or errors associated with recoil protons stopping in dead layers within the tagger – that lead to ambiguities in neutron energy and scattering angle. Combining all effects in Table I and summing uncertainties in quadrature, the net correction ( $\prod c_i$ ) applied to raw cross sections is  $\approx 1.10 \pm 0.015$ , with an angle-dependence of the systematic uncertainty indicated by the shaded band in Fig. 4.

The present results are in quite good absolute agreement with the Nijmegen PWA93 calculations, over the full angular range covered. The small deviations seen might be removed by minor tuning of phase shifts. In contrast, the present results deviate systematically, especially in the steepness of the back-angle cross section rise, from earlier measurements [2, 3] that the Nijmegen group had rejected in their analyses by applying controversial criteria. These deviations are larger than the differences expected from the neutron energy changes among the various experiments. As the back-angle rise is particularly influential in pole extrapolations used [8, 12] to extract the pion-nucleon-nucleon coupling constant, the present data strongly favor the value ( $f_c^2 = 0.0748 \pm 0.0003$ ) given by the Nijmegen [6] and other [5] partial-wave analyses.

We thank the operations staff of the Indiana University Cyclotron Facility for providing the superior quality cooled beams, and Hal Spinka and Catherine Lechanoine-

TABLE I: Correction factors ( $c_i$ ) and systematic uncertainties in correction factors for the np cross sections.

Source	Correction Factor	Uncertainty
Accid. tagger coinc.	1.0003	$< \pm 0.001$
Non-D <sub>2</sub> tagger background	1.0067 (2-stop); 1.0044 (1-punch)	$\pm 0.002$
n pos'n unc. on CH <sub>2</sub>	1.0000	$\pm 0.001$
n atten'n before CH <sub>2</sub>	1.005	$\pm 0.0025$
C bkgd. subtraction	1.0000	$\pm 0.004$
Reaction tail losses	1.004	$\pm 0.002$
Neutron polarization effects	Angle-dependent: > 0.9988 (1-punch) < 1.0014 (2-stop)	$\pm 0.001$
Software cut losses	1.010	$\pm 0.005$
Sequential react'ns & $x_{tag}(n)$ errors	1.063	$\pm 0.010$
CH <sub>2</sub> tgt. thickness	1.0000	$\pm 0.004$
np scattering acceptance	1.0000	$\leq \pm 0.001$ ( $> 120^\circ$ ) $\rightarrow \pm 0.017$ ( $90^\circ$ )
MWPC efficiency	1.017	$\pm 0.002$
Trigger inefficiency	$1.002 + 0.008 \times \cos^2(\theta_p^{LAB})$	$\pm [0.001 + 0.004 \times \cos^2(\theta_p^{LAB})]$
Dead time diffs.	0.991	$\pm 0.005$
Scattering angle errors	1.000	angle-dependent, $\leq \pm 0.004$
Corruption subt'n	1.000	$< \pm 0.001$
<b>Net</b>	$\approx 1.10$	$\approx \pm 0.015$

Leluc for the loan of critical detector hardware, needed for successful execution of this experiment. We acknowledge the U.S. National Science Foundation's support under grant numbers NSF-PHY-9602872 and 0100348.

\* Present address: Dept. of Radiology and Radiological Sciences, Vanderbilt University, Nashville, TN, USA

† Present address: Dept. of Physics, University of Zagreb, Zagreb, Croatia

- [1] B.E. Bonner *et al.*, Phys. Rev. Lett. **41**, 1200 (1978).
- [2] J. Franz *et al.*, Phys. Scr. **T87**, 14 (2000).
- [3] J. Rahm *et al.*, Phys. Rev. **C57**, 1077 (1998).
- [4] V. Stoks *et al.*, Phys. Rev. **C48**, 792 (1993).
- [5] D.V. Bugg and R. Machleidt, Phys. Rev. **C52**, 1203 (1995).
- [6] M.C.M. Rentmeester, R.G.E. Timmermans and J.J. deSwart, Phys. Rev. **C64**, 034004 (2001).
- [7] M.C.M. Rentmeester *et al.*, Phys. Rev. Lett. **81**, 5253 (1998); T.E.O. Ericson *et al.*, *ibid.*, 5254 (1998).
- [8] Proc. Workshop on *Critical Issues in the Determination of the Pion-Nucleon Coupling Constant*, ed. J. Blomgren, Phys. Scr. **T87** (2000).
- [9] J.J. de Swart and R.G.E. Timmermans, Phys. Rev. **C66**, 064002 (2002).
- [10] T. Peterson *et al.*, Nucl. Instr. Meth. **A527**, 432 (2004).
- [11] R.E. Pollock, Annu. Rev. Nucl. Part. Sci. **41**, 357 (1991).
- [12] T.E.O. Ericson *et al.*, Phys. Rev. Lett. **75**, 1046 (1995).
- [13] <http://nn-online.sci.kun.nl/NN/>